Supporting Information

1. Shallow water model

The shallow water model is based on the Athena++ modeling framework (1), adapted to simulating planetary atmospheres (2). The prognostic variables are (u, v, ϕ), where $\phi = gh$. The velocities, (u, v) are chosen to fit the observational values from the Juno/JIRAM. The far-field value of ϕ (ϕ_0) is uncertain, and we explored them via the Burger number $Bu = \frac{\phi_0}{(fL)^2}$, where $f = 2\Omega = 3.48 \times 10^{-4}\ \mathrm{s}^{-1}$ is the Coriolis parameter and L is the length scale of interest, which we choose to be the radius of the vortex (defined later). We have explored the range of Bu from 1 to 1000, corresponding to a range of deformation radius $L_d = \frac{\sqrt{\phi_0}}{f}$, from 10^3 km to 3.1×10^4 km.

The computational domain is a square domain of 7×10^4 km wide centered at the pole. The middle of the sides of the square is located at approximately 61 degrees in latitude. Sponge layers, starting at 65° latitude and outward, are applied at four sides and coners to mitigate the boundary effects. Velocities are damped at a constant rate and with increasing strength outside of the 65° latitude circle. We use 512×512 resolution, with each computational cell being 136 km wide, which is about 10 times smaller than the size of the vortices. The model is discretized using the finite volume method with (u, v, ϕ) being all at collocated positions. The advective fluxes are calculated using a Shallow Water Riemann Solver (3) and the time integration is performed by third-order Strong Stability Preserving Runga-Kutta scheme (4).

We initialize our model by placing a family of vortices in the observed geometry at the south pole – one cyclone at the pole surrounded by 5 other cyclones of the size and strength. Some experiments have another cyclone – an intruder – near the edge of the computational domain to study the impact of an outside intruder. The intruder will drift toward the pole due to the beta effect and interact with the original family of vortices. The initial velocity of each vortex is calculated according to equation (1) in the main manuscript, which depends on the maximum azimuthal velocity (v_m), the radius (r_m) it is achieved, and the steepness parameter b. In the model, we fix $r_m = 10^3$ km, and vary v_m according to the Rossby number defined as $Ro = \frac{v_m}{f r_m}$. We use $Ro = 0.2$ for most of our experiments. Using the incomplete gamma function $\Gamma(s, x) = \int_x^\infty t^{s-1} e^{-t} \mathrm{d}t$, the initial geopotential field (ϕ) of each vortex has an analytical solution given the geostrophic balance if f is assumed to be constant:

$$\begin{aligned} \phi(r) &= \phi_0 - \int_r^\infty \left(\frac{v^2}{r} + fv \right) \mathrm{d}r \\ &\approx \phi_0 \left(1 - \frac{Ro}{Bu} e^{\frac{1}{b}} b^{\frac{2}{b}-1} \Gamma\left(\frac{2}{b}, \frac{1}{b} \left(\frac{r}{r_m} \right)^b \right) \right). \end{aligned} \tag{1}$$

Then, both initial geopotential and the initial velocities are calculated by linearly adding contributions from all vortices. Although this method is only approximately correct for generating a balanced geopotential/velocity field, we find no discernable gravity waves after the model started (movied provided online). Each numerical experiment is integrated for more than 500 Earth days, at which the whole structure stabilizes. Since our experiment setting is an initial value problem without continuous forcing, the numerical dissipation will eventually destroy all vortices if integrated indefinitely. We have refined our model resolution until a semi-steady state can be achieved after several hundreds of days given that the observations are taken every 53 days.

2. Vortex shielding

The steepness parameter b is a crucial quantity determining whether cyclones are shielded or not. The distribution of potential vorticity (PV) of a vortex is define as:

$$\begin{aligned} PV(r) &= \frac{1}{\phi(r)}\left(f + \frac{v}{r} + \frac{\partial v}{\partial r}\right) \\ &= \frac{f}{\phi_0}\frac{1 + Ro\left(2 - \left(\frac{r}{r_m}\right)^b\right)\exp\left(\frac{1}{b}\left(1 - \left(\frac{r}{r_m}\right)^b\right)\right)}{1 - \frac{Ro}{Bu}e^{\frac{1}{b}}b^{\frac{2}{b}-1}\Gamma\left(\frac{2}{b}, \frac{1}{b}\left(\frac{r}{r_m}\right)^b\right)}. \end{aligned} \tag{2}$$

PV shielding occurs when the relative vorticity becomes anticyclonic at some radius r and therefore $PV(r) < \frac{f}{\phi_0}$:

$$\frac{1 + Ro\left(2 - \left(\frac{r}{r_m}\right)^b\right)\exp\left(\frac{1}{b}\left(1 - \left(\frac{r}{r_m}\right)^b\right)\right)}{1 - \frac{Ro}{Bu}e^{\frac{1}{b}}b^{\frac{2}{b}-1}\Gamma\left(\frac{2}{b}, \frac{1}{b}\left(\frac{r}{r_m}\right)^b\right)} < 1, \tag{3}$$

which leads to the condition:

$$Bu\left(\left(\frac{r}{r_m}\right)^b - 2\right)\exp\left(\frac{1}{b}\left(1 - \left(\frac{r}{r_m}\right)^b\right)\right) > e^{\frac{1}{b}}b^{\frac{2}{b}-1}\Gamma\left(\frac{2}{b}, \frac{1}{b}\left(\frac{r}{r_m}\right)^b\right). \tag{4}$$

At small radius $\left(r < 2^{1/b}r_m\right)$, the above condition does not satisfy. At larger radius, the above condition can be satisfied only if:

$$Bu > \min\left\{\frac{b^{\frac{2}{b}-1}e^{\frac{1}{b}\left(\frac{r}{r_m}\right)^b}\Gamma\left(\frac{2}{b}, \frac{1}{b}\left(\frac{r}{r_m}\right)^b\right)}{\left(\frac{r}{r_m}\right)^b - 2}\right\} = Bu^*. \tag{5}$$

When $b > 1$, $Bu^* = 0$, which means that all vortices with $b > 1$ will be shielded eventually although it may occur at greater distance. When $b < 1$, the value of Bu^* as a function of b is displayed in Figure S1. A larger value of Bu allows a wider range of b for shielding. In the strictly 2D limit, $Bu \to \infty$, all vortices regardless of the value of b will be shielded and that's probably why vortex crystals are often observed in numerical simulations using the 2D Euler equations (5, 6). In the adiabatic limit, $Bu \to 0$, only vortices with $b > 1$ can be shielded. If the atmospheric motion is unable to generate such kind of vortex, vortices are deemed to merge in interaction as many shallow water studies have shown with small values of Bu. Therefore we conclude that a larger value of Bu is conducive for vortex separation.

3. Movies of numerical experiments

We provide all movies of the numerical experiments we have performed. The file names, parameters and their behavior are summarized in Table S1. The movie files are accessible at the webpage

https://github.com/chengcli/2020.JupiterPolarVortex/tree/master/movies. Specifically, the following experiments showcase the parameter space we have explored.

1) Intruder experiment

The experiment with $Ro = 0.23, b = 1.5, Bu = 10$ simulates the condition of Jupiter's poles (Figure 4 in the main manuscript and movie here). The intruder drifts toward the pole but does not merge with the original family of vortices. As the intruder migrates, part of its anticyclonic shielding strips off and forms a small anticyclone that drifts out of the domain due to the same beta effect. Another part of its anticyclonic shielding was initially taken by the vortex at 4 o'clock and subsequently traveled through all cyclones at the peripheral. The intruder re-absorbed most of the traveling anticyclone patch at later times and join the original family of vortices to form a hexagon in the end. The Juno/JIRAM instrument observed a similar transition from pentagon to hexagon but the new vortex was soon pushed out.

https://github.com/chengcli/2020.JupiterPolarVortex/blob/master/movies/R10Bu10b1p5.mp4?raw=true

2) Merging experiment

The experiment with $Ro = 0.2, b = 1, Bu = 2$ demonstrates vortices merge if shielding is weak. Vortices start to merge at $t = 205$ days and all vortices merge into a single polar cyclone at day 638.

https://github.com/chengcli/2020.JupiterPolarVortex/blob/master/movies/int_Bu1bp8.mp4?raw=true

3) Tripole formation

As b increases, the anticyclonic shielding becomes unstable and forms tripoles. For example, the experiment with $Ro = 0.2, b = 3, Bu = 1$ demonstrates the formation of tri-polar vortices. The axisymmetric shielding becomes unstable shortly after the simulation started. The original anticyclonic padding breaks into two anticyclonic satellite vortices orbiting 180° apart around the central one. The whole structure remains stable with the presence of tripoles.

https://github.com/chengcli/2020.JupiterPolarVortex/blob/master/movies/R10Bu1b3.mp4?raw=true

4) Clash of tripoles

As Bu increases, the vortices migrate to the pole at a faster rate, which may lead to a clash of tripoles. The experiment with $Ro = 0.2, b = 3, Bu = 10$ demonstrates the clash and the reformation of an axisymmetric shielding structure. The vortices bounce each other as if they are rigid balls. They equilibrated at a distance larger than their minimum achieved distance.

https://github.com/chengcli/2020.JupiterPolarVortex/blob/master/movies/R10Bu10b3.mp4

5) Vortex disintegrating

The most extreme case occurs when both b and Bu are large. We only tried two cases with $b = 4$. In the case of $b = 4, Bu = 2$, the initial 5 vortices split into 10 vortex pairs with each having a cyclone and an anticyclone. Close inspection of the movie shows that tripoles formed first and then the central cyclone was pulled apart by its two anticyclonic satellites.

https://github.com/chengcli/2020.JupiterPolarVortex/blob/master/movies/R10Bu2b4.mp4?raw=true

Reference

1. C. J. White, J. M. Stone, C. F. Gammie, An Extension of the Athena++ Code Framework for GRMHD Based on Advanced Riemann Solvers and Staggered-mesh Constrained Transport. *Astrophys. J. Suppl. Ser.* **225**, 22 (2016).

2. C. Li, X. Chen, Simulating Nonhydrostatic Atmospheres on Planets (SNAP): Formulation, Validation, and Application to the Jovian Atmosphere. *Astrophys. J. Suppl. Ser.* **240**, 37 (2019).

3. R. J. LeVeque, *Finite volume methods for hyperbolic problems* (Cambridge university press, 2002).

4. S. Gottlieb, D. I. Ketcheson, C.-W. Shu, *Strong stability preserving Runge-Kutta and multistep time discretizations* (World Scientific, 2011).

5. D. A. Schecter, D. H. E. Dubin, K. S. Fine, C. F. Driscoll, Vortex crystals from 2D Euler flow: Experiment and simulation. *Phys. Fluids* **11**, 905–914 (1999).

6. J. Jiménez, A. Guegan, Spontaneous generation of vortex crystals from forced two-dimensional homogeneous turbulence. *Phys. Fluids* **19**, 085103 (2007).

Movie Legends

Movie S1: Case with $Bu = 10,\ b = 1.5$.

Movie S2: Case with $Bu = 2,\ b = 1.0$.

Movie S3: Case with $Bu = 1,\ b = 1.5$.

Movie S4: Case with $Bu = 1,\ b = 2.25$.

Movie S5: Case with $Bu = 1,\ b = 3$.

Movie S6: Case with $Bu = 1,\ b = 3.75$.

Movie S7: Case with $Bu = 10,\ b = 3$.

Movie S8: Case with $Bu = 2,\ b = 4$.

Movie S9: Case with $Bu = 5,\ b = 4$.

Table S1: Summary of experiments.

file name	b	Bu	Ro	r_m (km)	V_m (m/s)	phi0 (m^2/s^2)	behavior
R10Bu1bp75	0.75	1	0.2	1.00E+06	69.6	1.19E+05	merger
R10Bu1b1	1	1	0.2	1.00E+06	69.6	1.19E+05	merger
R10Bu1b1p3	1.15	1	0.2	1.00E+06	69.6	1.19E+05	no tripoles
R10Bu1b1p5	1.5	1	0.2	1.00E+06	69.6	1.19E+05	no tripoles
R10Bu1b1p8	1.8	1	0.2	1.00E+06	69.6	1.19E+05	no tripoles
R10Bu1b2	2	1	0.2	1.00E+06	69.6	1.19E+05	no tripoles
R10Bu1bp2p25	2.25	1	0.2	1.00E+06	69.6	1.19E+05	tripoles
R10Bu1bp3	3	1	0.2	1.00E+06	69.6	1.19E+05	tripoles
R10Bu1bp3p75	3.75	1	0.2	1.00E+06	69.6	1.19E+05	tripoles
R10Bu1b4	4	1	0.2	1.00E+06	69.6	1.19E+05	tripoles
R10Bu2bp55	0.55	2	0.2	1.00E+06	69	2.38E+05	merger
R10Bu2b1	1	2	0.2	1.00E+06	69	2.38E+05	merger
R10Bu2b1p15	1.15	2	0.2	1.00E+06	69.6	2.38E+05	no tripoles
R10Bu2b1p8	1.8	2	0.2	1.00E+06	69.6	2.38E+05	no tripoles
R10Bu2b2	2	2	0.2	1.00E+06	69	2.38E+05	tripoles
R10Bu2b3	3	2	0.2	1.00E+06	69.6	2.38E+05	tripoles
R10Bu2b3p75	3.75	2	0.2	1.00E+06	69.6	2.38E+05	lost tripoles
R10Bu2b4	4	2	0.2	1.00E+06	69	2.38E+05	split
R10Bu5bp8	0.8	5	0.2	1.00E+06	69.6	5.97E+05	merger
R10Bu5b1	1	5	0.2	1.00E+06	69.6	5.97E+05	no tripoles
R10Bu5b3	3	5	0.2	1.00E+06	69.6	5.97E+05	lost tripoles
R10Bu5b3p75	3.75	5	0.2	1.00E+06	69.6	5.97E+05	split
R10Bu5b4	4	5	0.2	1.00E+06	69.6	5.97E+05	split
R10Bu10bp75	0.75	10	0.2	1.00E+06	69.6	1.19E+06	merger
R10Bu10b1	1	10	0.2	1.00E+06	69.6	1.19E+06	no tripoles
R10Bu10b1p5	1.5	10	0.2	1.00E+06	69.6	1.19E+06	no tripoles
R10Bu10b1p8	1.8	10	0.2	1.00E+06	69.6	1.19E+06	no tripoles
R10Bu10b2	2	10	0.2	1.00E+06	69.6	1.19E+06	tripoles
R10Bu10bp2p25	2.25	10	0.2	1.00E+06	69.6	1.19E+06	tripoles
R10Bu10bp3	3	10	0.2	1.00E+06	69.6	1.19E+06	lost tripoles
R10Bu10bp3p75	3.75	10	0.2	1.00E+06	69.6	1.19E+06	split
R10Bu20bp6	0.6	20	0.2	1.00E+06	69.6	2.39E+06	merger
R10Bu20bp7	0.7	20	0.2	1.00E+06	69.6	2.39E+06	merger
R10Bu20bp8	0.8	20	0.2	1.00E+06	69.6	2.39E+06	no tripoles
R10Bu100bp6	0.6	100	0.2	1.00E+06	69.6	1.19E+07	merger
R10Bu100bp8	0.8	100	0.2	1.00E+06	69.6	1.19E+07	no tripoles
R10Bu100b1	1	100	0.2	1.00E+06	69.6	1.19E+07	no tripoles
R10Bu1000b1	1	1000	0.2	1.00E+06	69.6	1.19E+08	no tripoles
int_Bu2b1	1	2	0.23	1.00E+06	80	2.38E+05	no polygon
int_Bu10b1p5	1.5	10	0.23	1.00E+06	80	1.19E+06	polygon

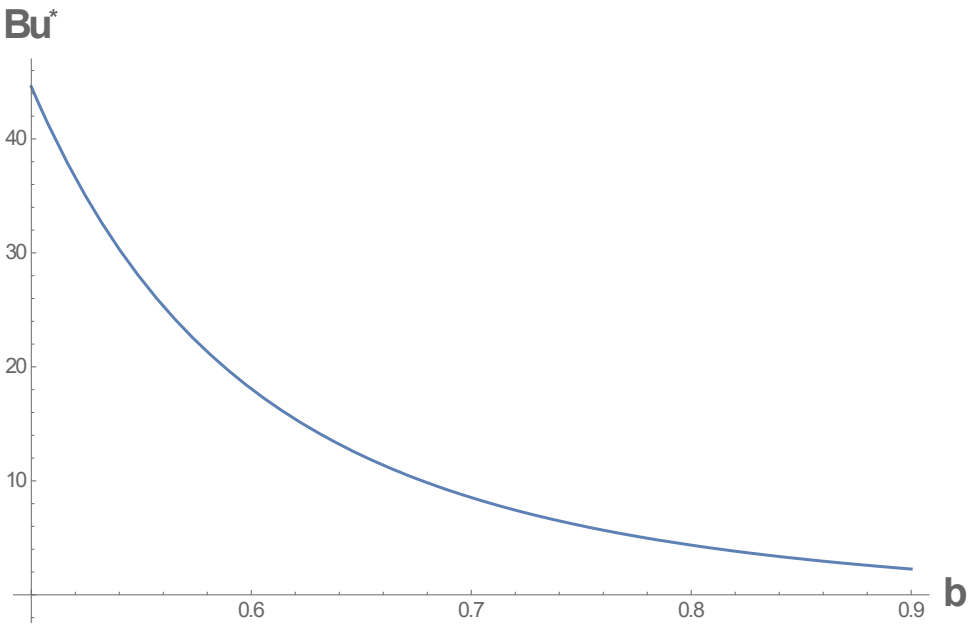

Figure S1. Critical curve Bu^* as a function of b